Substrate integrated waveguide filter-amplifier design using active coupling matrix technique

Gao, Yang; Zhang, Fan; Lv, Xin; Guo, Cheng; Shang, Xiaobang; Li, Lei; Liu, Jiashan; Liu, Yuhuai; Wang, Yi; Lancaster, Michael J.

DOI:
10.1109/TMTT.2020.2972390

Substrate Integrated Waveguide Filter Amplifier Design using Active Coupling Matrix Technique

Yang Gao, Fan Zhang, Xin Lv, Cheng Guo, Xiaobang Shang, Lei Li, Jiashan Liu, Yuhuai Liu, Yi Wang, *IEEE, Senior Member,* and Michael J. Lancaster, *IEEE, Senior Member*

***Abstract*—This paper presents a comprehensive active *N*+4 coupling matrix approach for the design of integrated filter-amplifiers. The feedback between gate and drain which is neglected in previously work is considered, which improves the accuracy of the coupling matrix model for transistors. More importantly, the relationship between the coupling matrix and the noise figure is also established, which extends the coupling matrix method to tackle noise related circuit functions. Substrate integrated waveguide (SIW) filters are used to implement an integrated X-band filter-amplifier design and to validate the design approach in terms of return loss, gain and noise. Compared with rectangular waveguide, SIW is utilized for its appealing advantages such as lower production cost, easier fabrication, and most importantly easier integration with active components. A second-order filtering circuit is applied to match simultaneously the input and output of the transistor. The integration reduces the losses from the intermediate networks in conventional designs, which is particularly important when the frequencies go higher. The measurements agree very well with the simulations in terms of S-parameters, gains and noise figures.**

***Index Terms*—Active coupling matrix, transistor, resonator, SIW filter amplifier.**

I. Introduction

AMPLIFIERS are essential components in a variety of microwave communication and radar systems [1]-[3]. Amplifiers and filters are usually constructed separately refer to 50-Ω impedance interface, and then cascaded in the system. For conventional amplifiers, matching networks are required to transfer the complex impedance of the transistor to 50-Ω. Widely used matching networks include stubs, quarter wavelength transformers, and coupled lines [4]; and specific examples can be found using single coplanar waveguide (CPW) line stubs [5], step ridges [6], and antipodal fin-line arrays [7]. These designs are based on independent transistors and the matching networks, which can suffer from additional loss, extra cost, and large circuit footprint.

To overcome the ohmic loss caused by the planar matching circuit as frequencies go higher, various low-loss 3-D waveguide structures have been used in millimeter-wave and sub-millimeter wave applications. Among them, SIW components are prevalently applied mainly due to their advantages of high Q-factors (low loss). Besides, their properties of low cost, compactness and easy manufacture have also attracted considerable attention, leading to the widespread use of SIW [8]-[11]. There has been extensive study of passive SIW components, such as filters [9]-[11], antennas [12], transitions [13], couplers [14], and power dividers [15]. Integration on of SIW technology with active devices, however, has not progressed as rapidly. Most SIW components are designed separately such as the antenna, filter, transition and amplifier components in [16]-[20].

Here, the SIW filters and the amplifier are integrated in a more compact manner to form the filter-amplifier, yielding reduced loss, simplified circuit structure, and reduced device volume. Fig. 1 illustrates the two approaches of filter-amplifier integration: Fig. 1(a) is the conventional amplifier cascaded with filters, where the input matching network (IMN) and output matching network (OMN) are employed to attain the 50-Ω ports. In Fig. 1(b), the matching networks (IMN and OMN) are replaced by the input and output matching filters in the amplifier. This integrated filter-amplifier can be schematically represented using a coupling topology in Fig. 1(c). Here the triangle denotes the transistor, the black circles denote the resonators and the white circles denote the source and load. It is very important to note that there exists feedback coupling between the input and output of the transistor. This has been neglected in all the previous treatment of filter-amplifier integration [21]-[24].

A few attempts have been made on the co-design of SIW filter-amplifiers [20]-[22]. In [20], SIW-based filter was combined with the amplifier to suppress up to the fourth harmonic. In [21] and [22], SIW filters were integrated at the

Manuscript received September 30, 2019; revised December 09, 2019; accepted January 5, 2020. This work is supported by the UK Engineering and Physical Science Research Council (EPSRC) under Contract EP/S013113/1 and the National Natural Science Foundation of China under Grant No. 61176008. (*Corresponding author Yi Wang; Yang Gao*).

Y. Gao and L. Li are with the School of Physics (Microelectronics), Zhengzhou University, Zhengzhou, 450052, China. (e-mail: gaoyang678@outlook.com).

F. Zhang is with School of Physics, University of Electronic Science and Technology of China, Chengdu, 610054, China.

X. Lv and J. Liu are with Beijing Key Laboratory of Millimeter Wave and Terahertz Technology, Beijing Institute of Technology, Beijing, 100089, China.

C. Guo is with the Department of Information and Communication Engineering, Xi'an Jiaotong University, Xi'an 710049, China.

X. Shang is with the National Physical Laboratory, Teddington, TW11 0LW, U.K.

Y. Liu is with National center for International Joint Research of Electronic Materials and Systems, School of Information Engineering, Zhengzhou University, Zhengzhou, 450052, China.

Y. Wang, Y. Gao and M. J. Lancaster are with the Department of Electronic, Electrical and Systems Engineering, University of Birmingham, Birmingham B15 2TT, U.K. (y.wang.1@bham.ac.uk, m.j.lancaster@bham.ac.uk).

Color versions of one or more of the figures in this paper are available online at http://ieeexplore.ieee.org.

Digital Object Identifier XXXXXXXXXXX

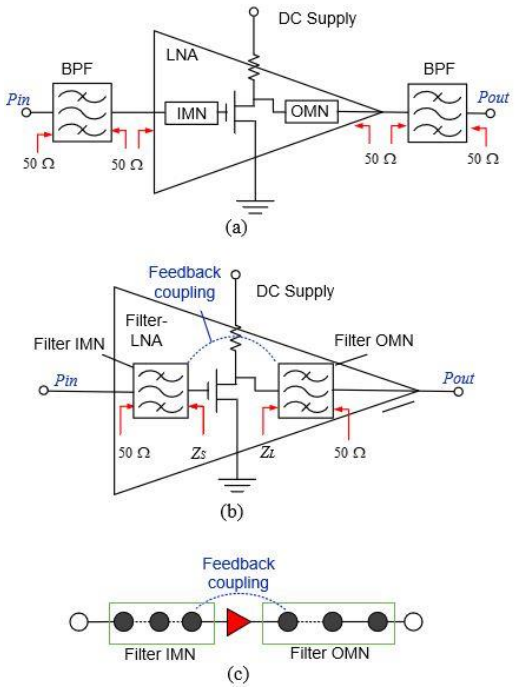

Fig. 1. (a) Conventional cascaded filters and amplifier with 50 Ω interfaces between them; (b) The proposed integrated filter-amplifier, with feedback coupling between the drain and gate; (c) The coupling topology representation of (b).

output of the transistor and Chebyshev filter response was achieved. Integrated waveguide filter amplifiers were reported in [23] and [24]. The filter was only coupled to the input of the transistor in [23]. This work was followed by [24] where filters are integrated at both the input and output of the amplifier. Most previous work only incorporates filters to match transistors at either the input or output. However, as a more general case, transistors can be integrated with filters on both sides, which is what we have achieved here.

In this paper, an *N*+4 active coupling matrix is developed and applied in the design of SIW integrated filter-amplifiers. Different from the previous filter-amplifiers, this work (i) reports the use of a new *N*+4 active matrix, which, for the first time, includes the feedback of the transistor (ii) also, for the first time, this paper derives the equations to calculate noise figures directly using the active coupling matrix; (iii) implemented the design using SIW, which allows easier integration with active circuits compared to the previous work using waveguides [23], [24]. Primary specifications regarding return loss, gain, as well as noise figure can be described and predicted by the newly derived *N*+4 coupling matrix.

Compared with the previous coupling matrix approach in [23] and [24], this new matrix formulation makes a more accurate representation of the transistors, as the input and output filter as well as the feedback coupling are considered as an entity. Without the feedback coupling, classic passive coupling matrix synthesis [25] and previous active coupling matrix [23], [24] are not able to predict amplifier responses precisely. For example, the simulated return loss from the initial extracted physical dimensions is only about 5 dB in the

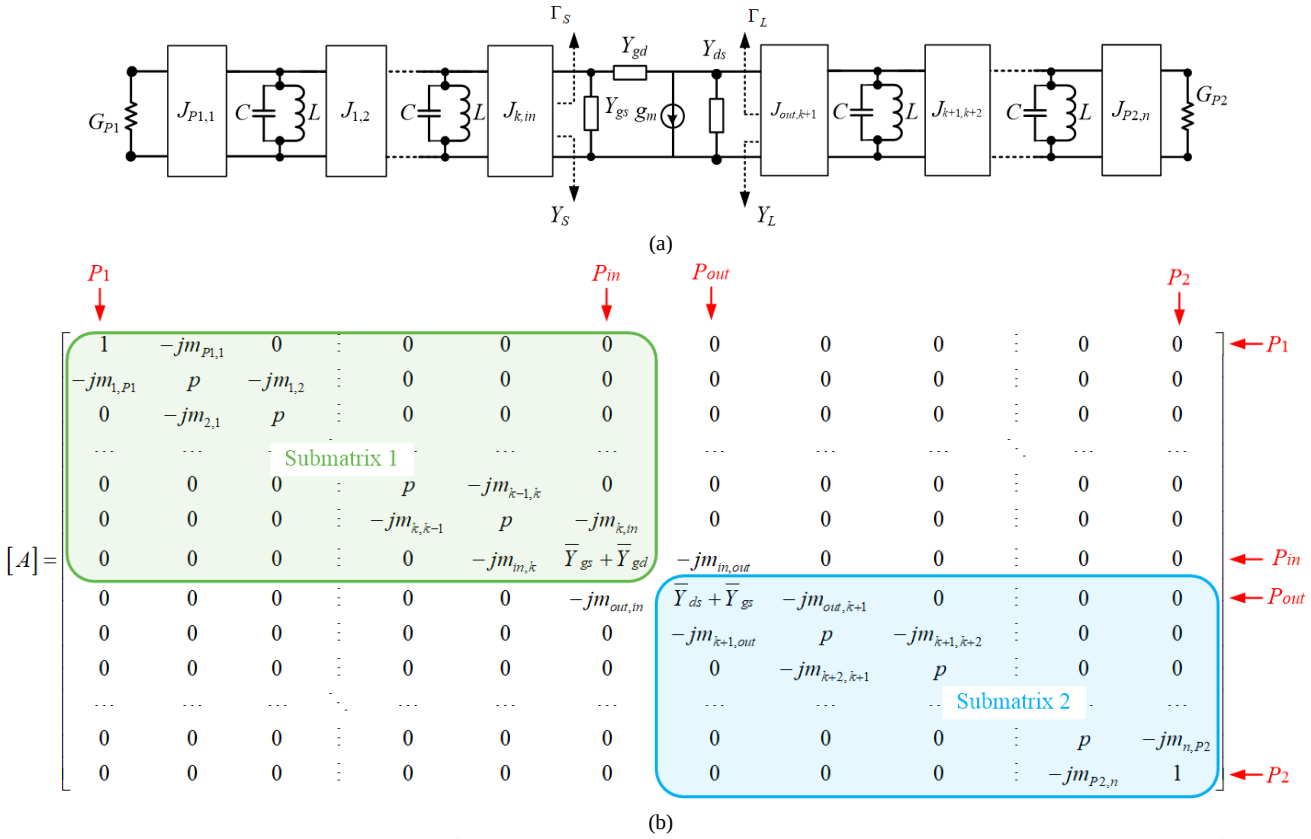

Fig. 2. Lumped equivalent circuit and coupling matrix of the transistor with input and output resonators matching. (a) Schematic representation of the circuit. (b) Coupling matrix representation of the filter-amplifier.

passband in [24], whereas in our new work this is about 12.5 dB, which is much closer to the 20 dB return loss specification. These more accurate initial values of the model facilitate the final EM optimization of the filter-amplifier. This greatly improves the design efficiency. For the *N*+4 active coupling matrix, a matrix optimization method based on local gradient algorithm is applied. An effective procedure for filter dimension extraction is implemented using an example of an X-band filter-amplifier.

This paper is organized as follows. Section II introduces the concept of the new *N*+4 active coupling matrix, where its relationship with noise figure is derived. Section III presents the optimization of *N*+4 matrix using a local gradient optimization algorithm to produce Chebyshev response. Section IV describes the physical design using the *N*+4 coupling matrix, with a prototype X-band SIW amplifier-filter. This is followed by the fabrication and the measurement results in Section V. The conclusions and discussions are in Section VI.

II. The Active *N*+4 Coupling Matrix

The lumped circuit representation of resonators matching the input and output of the transistor is illustrated in Fig. 2(a). The parallel *LC* resonators are coupled through *J* inverters. There are *N* resonators in total: the k^{th} resonator is coupled to the input of the transistor at the gate and the $(N\text{-}k)^{\text{th}}$ resonator is coupled to the drain at the output of the transistor. G_{P1} and G_{P2} are the source and load conductance; Y_{gs}, Y_{gd}, and Y_{ds} are the admittances between the transistor's gate, source and drain, and g_m is the transconductance. Y_S is the input admittance seen by the source and Y_L is the input admittance seen by the load. By applying Kirchoff's laws in the lumped circuit in Fig. 2(a) and the matrix scaling process described in [25], the active *N*+4 coupling matrix can be constructed [24] and is illustrated in Fig. 2(b). This *N*+4 active coupling matrix is normalized to a 1-Ω system as the port admittance is taken as 1. *p* is the complex frequency variable defined as [22]

$$p = j\frac{1}{FBW}\left(\frac{\omega}{\omega_0}-\frac{\omega_0}{\omega}\right) \tag{1}$$

There are two submatrices in Fig. 2(b) corresponding to the input and output matching filters. $\bar{Y}_{gs}$, $\bar{Y}_{gd}$, $\bar{g}_m$ and $\bar{Y}_{ds}$ are the normalized parameters. $m_{i,j}$ is the inter-resonator coupling and $m_{P1,1} = m_{1,P1}$ and $m_{P2,4} = m_{4,L}$ are the external couplings from the resonators to the source and load. The self-coupling $m_{i,i}$ results from a frequency offset of the resonator *i* from the central frequency of the circuit, $m_{2,in} = m_{in,2}$ and $m_{out,3} = m_{3,out}$ are the couplings between the transistor's gate or drain with its adjacent resonator. $m_{in,out}$ and $m_{out,in}$ are the couplings between the transistor's input and output and are given in terms of the normalized transistors parameters as [19],

$$m_{in,out} = \frac{\bar{Y}_{gd}}{j}, m_{out,in} = \frac{\bar{Y}_{gd}-\bar{g}_m}{j} \tag{2}$$

Matrix [*A*] in Fig. 2(b) can be further decomposed into three matrices [26]

$$[A] = [T] + p\cdot[U] - j\cdot[m] \tag{3}$$

where the [*T*] contains the filter's port admittances and the input and output admittance of the transistor. [*U*] is the identity matrix except for entries $U_{P1,P1}$, $U_{in,in}$, $U_{out,out}$ and $U_{P2,P2}$, which are zero. *m* is the coupling matrix with elements discussed above.

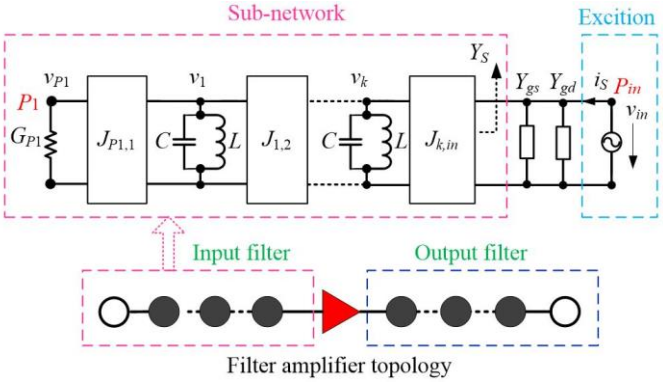

Fig. 3. Lumped circuit sub-network representation of the input filter.

The *S*-parameters for the complete filter-amplifier circuit can be calculated using [25], [27]

$$\begin{aligned} S_{11} &= 2[A]^{-1}_{P1,P1} - 1 \quad S_{12} = 2[A]^{-1}_{P1,P2} - 1 \\ S_{21} &= 2[A]^{-1}_{P2,P1} - 1 \quad S_{22} = 2[A]^{-1}_{P2,P2} - 1 \end{aligned} \tag{4}$$

The noise figure can also be calculated using the matrix [*A*] and the formulas are derived as follows.

Firstly, the matrix [*A*] is divided into submatrices corresponding the input and output filters. We use subscript *sub*1 to denote the submatrix 1 and *sub*2 as the submatrix 2, as shown in Fig. 2(b). The corresponding lumped circuit sub-network of the input filter, shown in Fig. 3, is extracted to help with the noise figure derivation. A current i_S is set up as an excitation source. The voltages at the nodes P_{in} and P_1 are denoted as v_{in} and v_{P1}; the voltage at the n^{th} resonator is denoted by v_n (n = 1 to k). Applying Kirchoff's law at each node, the following matrix form equations can be written:

$$\begin{bmatrix} G_{P1} & -jJ_{P1,1} & 0 & \text{L} & 0 & 0 \\ -jJ_{1,P1} & p' & -jJ_{1,2} & \text{L} & 0 & 0 \\ 0 & -jJ_{2,1} & p' & \text{L} & 0 & 0 \\ \text{M} & \text{M} & \text{M} & \text{O} & \text{M} & \text{M} \\ 0 & 0 & 0 & \text{L} & p' & -jJ_{k,in} \\ 0 & 0 & 0 & \text{L} & -jJ_{k,in} & Y_{gs}+Y_{gd} \end{bmatrix} \begin{bmatrix} v_{P1} \\ v_1 \\ 0 \\ \text{M} \\ v_k \\ v_{Pin} \end{bmatrix} = \begin{bmatrix} 0 \\ 0 \\ 0 \\ \text{M} \\ 0 \\ i_S \end{bmatrix} \tag{5}$$

or

$$[Y_{sub1}]\cdot[v] = [i] \tag{6}$$

where

$$p' = p\cdot\omega C\cdot FBW \tag{7}$$

The voltage at P_{in} can be calculated by

$$v_{Pin} = i_S\cdot[Y_{sub1}]^{-1}_{Pin,Pin} \tag{8}$$

Note that input admittance seen from the current source i_S is given by

$$\frac{i_S}{v_{in}} = Y_S + Y_{gs} + Y_{gd} \tag{9}$$

Substituting (8) for (9) yields

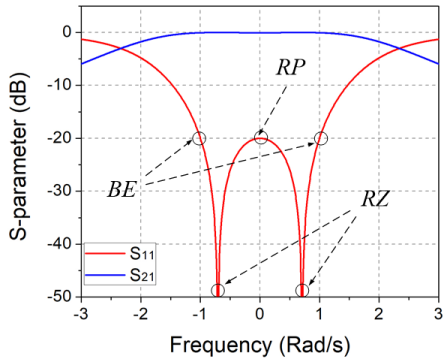

Fig. 4. The critical points of a filter having Chebyshev response.

$$Y_S = \frac{1}{\left[Y_{sub1}\right]^{-1}_{P_{in},P_{in}}} - Y_{gs} - Y_{gd} \tag{10}$$

The next step is to find the relationship between $[Y_{sub1}]$ and $[A_{sub1}]$. Note that in the lumped circuit in Fig. 2(a) and Fig. 3 the port admittances G_{P1} and G_{P2} are not normalized, whereas in coupling matrix $[A]$ of Fig. 2(b) the port admittances are normalized to identity. Applying narrow band approximation, $[A_{sub1}]^{-1}_{Pin,Pin}$ can be expressed by [25]

$$\left[A_{sub1}\right]^{-1}_{P_{in},P_{in}} = Y_0 \cdot \left[Y_{sub1}\right]^{-1}_{P_{in},P_{in}} \tag{11}$$

The input admittance seen into the source Y_S can be calculated by substituting (11) into (10), giving

$$Y_S = Y_0\left(\frac{1}{\left[A_{sub1}\right]^{-1}_{P_{in},P_{in}}} - \overline{Y}_{gs} - \overline{Y}_{gd}\right) \tag{12}$$

After Y_S is obtained, the noise figure can be calculated using the noise figure model [4],

$$NF = NF_{min} + \frac{R_N}{\mathrm{Re}\left[Y_S\right]}\left|Y_S - Y_{opt}\right|^2 \tag{13}$$

resulting in

$$NF = NF_{min} + \frac{R_N \cdot \left|Y_0\left(\frac{1}{\left[A_{sub1}\right]^{-1}_{P_{in},P_{in}}} - \overline{Y}_{gs} - \overline{Y}_{gd}\right) - Y_{opt}\right|^2}{\mathrm{Re}\left[Y_0\left(\frac{1}{\left[A_{sub1}\right]^{-1}_{P_{in},P_{in}}} - \overline{Y}_{gs} - \overline{Y}_{gd}\right)\right]} \tag{14}$$

Here, Y_{opt} is the optimum source admittance that results in minimum noise figure, NF_{min} is the minimum noise figure of the transistor that occurs when $Y_S = Y_{opt}$. R_N is the equivalent noise resistance of the transistor.

By incorporating the transistor parameters, the integrated filter-amplifier can be described using the active N+4 coupling matrix. Both the S-parameter response and the noise figure of the filter-amplifier can be calculated using the N+4 matrix.

III. The Active N+4 Matrix Optimization

Generally, the input and output impedances of the amplifier are complex. Previous research [21]-[23] showed that by adjusting the couplings strength and center frequency the input/output resonators can be matched to the complex impedance of the transistor. In [24], a more general case was presented, where the amplifier was matched at the input and output ports. However, the feedback between the gate and drain, represented as Y_{gd} in the models shown in Fig. 2 and Fig. 3, was neglected. In [24], the absence of Y_{gd} results in the inaccurate calculated gain and initial dimensions of the physical construction. Inclusion of the feedback coupling offers more accurate coupling matrix, nevertheless, presents a difficulty for the matching of the transistor.

To make a filter-amplifier with desired filtering response at both the input and output of the transistor, a local optimization method based on the gradient algorithm can be utilized. The coupling matrix $[m]$ can be produced achieving target response. The goal of the optimization is to minimize a scalar Cost Function (CF), by modifying the values of elements of $[m]$. The cost function is formulated to quantify the difference between the optimized results and the desired filter response. In this paper, we apply the Chebyshev filter as an example, but the technique can be generalized to other filter types. Some critical characteristic points are chosen to form the cost function, including the reflection zeros (RZ), the reflection poles within the pass-band (RP), and the equal-ripple passband edges (BE).

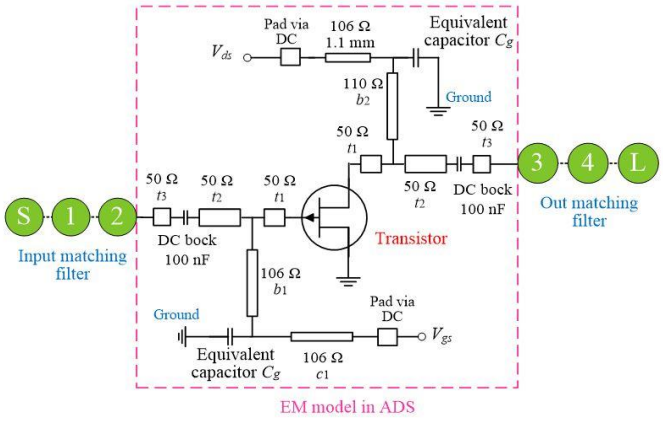

Fig. 5 On-chip transistor circuit schematic of the filter-amplifier.

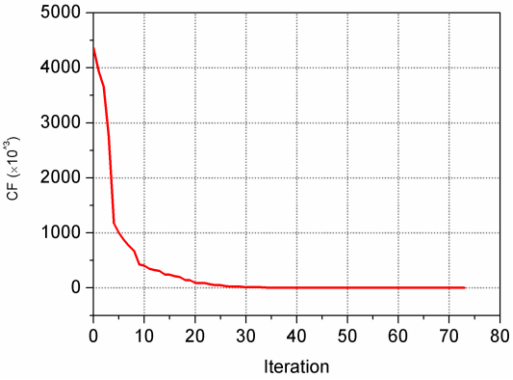

Fig. 6 Change of the cost function value with each iteration.

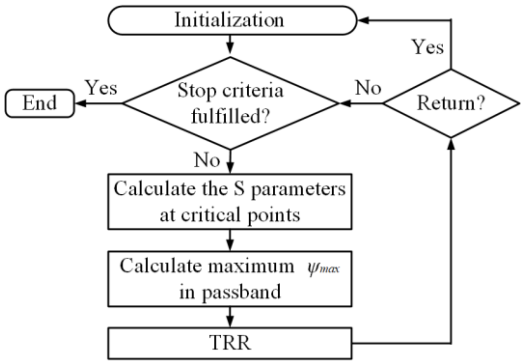

Fig. 7. Flowchart of matrix optimization procedure.

These are illustrated using a 2nd order filter with a Chebyshev response in Fig. 4. The cost function can be written as

$$\begin{aligned} CF = &\sum_{i=1}^{k} a_i \left|S_{11}(\Omega_{RZi})\right| + \sum_{i=1}^{2} b_i \left|\left|S_{11}(\Omega_{BEi})\right| - \varepsilon\right| \\ &+ \sum_{i=1}^{k-2} c_i \left|\left|S_{11}(\Omega_{RPi})\right| - \varepsilon\right| + \sum_{i=1}^{N-k} d_i \left|S_{22}(\Omega_{RZi})\right| \\ &+ \sum_{i=1}^{2} e_i \left|\left|S_{22}(\Omega_{BEi})\right| - \varepsilon\right| + \sum_{i=1}^{N-k-2} f_i \left|\left|S_{22}(\Omega_{RPi})\right| - \varepsilon\right| \\ &+ h\left|\left|\psi_{max}(\Omega)\right| - NF_{min}\right| \end{aligned} \tag{15}$$

where a_i, b_i, c_i, d_i e_i and h are the weights of each term, ε represents the maximum value of S_{11} in the passband. Note that, within the last term of (15), $\psi_{max}(\Omega)$ is defined as the maximum value of the achieved noise figure in passband during the iteration. Practically, the noise figure is calculated using (14), and its maximum evaluated. The cost function in (15) is a general case of the transistor coupled between two filters. A k^{th} order filter is matched at the transistor's input and the other $(N-k)^{th}$ order filter is coupled at the transistor's output. The gradient-based optimization function *fmincon* from MATLAB with the trust-region-reflective (TRR) algorithm is utilized for the optimization. It searches for the desired coupling matrix that minimizes the cost-function in (15). The coupling matrix is optimized for the desired impedance matching and noise matching or trade-off between them by assigning the weights of each term in the cost function. It should be noted that the same methodology can be applied to design other amplifiers with different performance requirements such as maximum power or constant specific gain. As with the case of noise figure, other parameters such as gain (related to S_{21}) and stability can also be expressed from the active coupling matrix and added to the cost function. This means the methodology is also applicable to power amplifier designs, which is an important and an interesting area for future work.

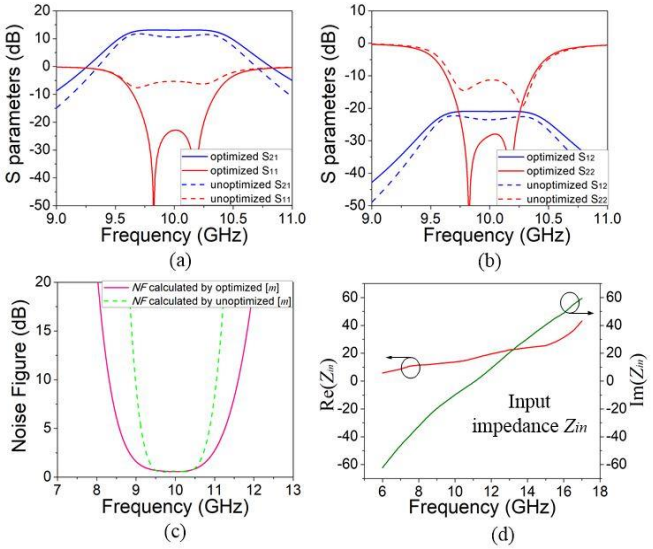

Fig. 8. Comparison of the calculated responses from the initial and the optimized coupling matrix. (a) S_{11} and S_{21}; (b) S_{22} and S_{12}; (c) Noise figure *NF*; (d) Input impedance of the transistor.

IV. Physical Design of Filter-Amplifier Based on the Coupling Matrix

A. Circuit Response Calculation using the Coupling Matrix

In our design example, k = 2 and N = 4, and two 2-pole Chebyshev filters are implemented at the gate and drain of the transistor. A center frequency f_0 of 10 GHz, a bandwidth of 500 MHz (fractional bandwidth FBW = 0.05), a passband equal-ripple return loss of 20 dB and the minimum noise figure of NF_{min} are targeted. The values of the coupling coefficients are produced using the N+4 coupling matrix optimization technique discussed in Section III.

Before pursuing the coupling matrix [m] calculation, the active entries in [m] related to the transistor should be found. The transistor is represented by the small signal lumped circuit [1] in Fig. 2(a). In order to get the accurate model of the

$$[m]_{opt} = \begin{bmatrix} 0 & 1.52 & 0 & 0 & 0 & 0 & 0 & 0 \\ 1.52 & 0 & 2.42 & 0 & 0 & 0 & 0 & 0 \\ 0 & 2.42 & 1.56 & 2.95 & 0 & 0 & 0 & 0 \\ 0 & 0 & 2.95 & 0 & -0.427-0.279j & 0 & 0 & 0 \\ 0 & 0 & 0 & -21.08-14.3j & 0 & 2.28 & 0 & 0 \\ 0 & 0 & 0 & 0 & 2.28 & -0.32 & 2.28 & 0 \\ 0 & 0 & 0 & 0 & 0 & 2.28 & 0 & 1.476 \\ 0 & 0 & 0 & 0 & 0 & 0 & 1.476 & 0 \end{bmatrix} \tag{16}$$

TABLE I
VALUES OF TRANSISTOR'S Y MATRIX PARAMETERS

Y parameters	Values	Normalized $\bar{Y}$ parameters	Values
g_m	0.0696- 0.1350j	$\bar{g}_m$	-13.435+20.677j
Y_{gd}	0.0003+ 0.0033j	$\bar{Y}_{gd}$	0.2673 - 0.4289j
Y_{ds}	0.0055+ 0.0127j	$\bar{Y}_{ds}$	2.1017 - 1.485j
Y_{gs}	0.0051+ 0.0276j	$\bar{Y}_{gs}$	2.3267 - 3.7277j

All parameters are calculated from the data sheet with the transistor operating at 10 GHz.

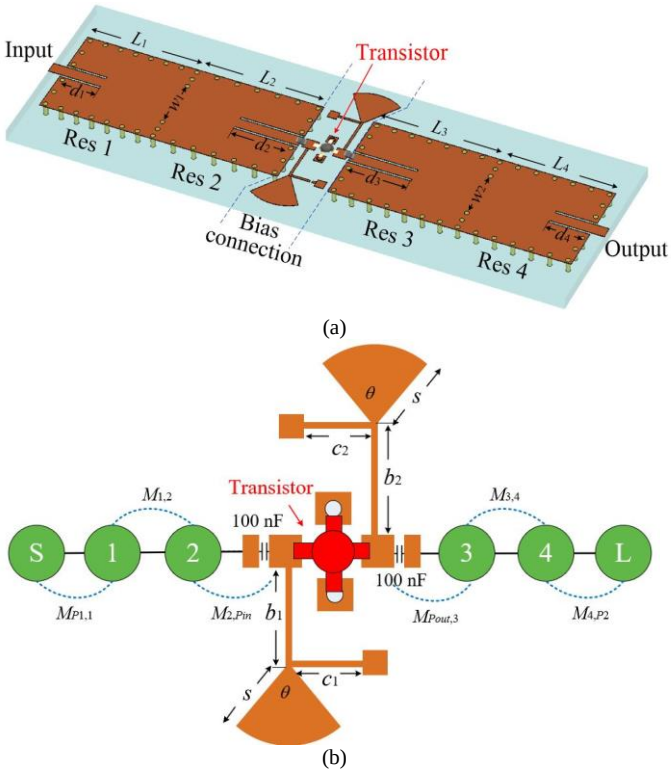

Fig. 9 (a) Physical layout of the SIW filter amplifier. (b) Schematic of the filter matching input and output of the transistor.

transistor, the on-chip microstrip board including the bias connection and dc-blocking capacitors are modeled in ADS. Fig. 5 shows the circuit schematic of transistor with bias tees. The transistor used is NES3210s01, and the parameters of the transistor are provided by the manufacturer [28]. Bias tees are realized by the high-impedance shorted transmission lines. Capacitors are used to block the dc-voltages. The transistor including bias connection is simulated in ADS, and the resultant S-parameters of S_{11} and S_{22} operating at 10 GHz center frequency are obtained. The simulated S-parameters can be employed to calculate the normalized admittance parameters [26], with results given in Table I.

According to the filter specification and the transistor's parameters in Table I, the N+4 coupling matrix [m] is optimized. Note that the feedback between gate and drain Y_{gd} is taken into account in this matrix. It is determined from the parameters of the transistor and kept constant during the optimization. The initial values provided to the optimisation algorithm are $m_{P1,1} = m_{1,P1} = 1.226$, $m_{1,2} = m_{2,1} = 1.662$, $m_{in,2} = m_{2,in} = 1.226$, $m_{out,3} = m_{3,out} = 1.226$, $m_{3,4} = m_{4,3} = 1.662$, $m_{P2,4} = m_{4,P2} = 1.226$. These are calculated from a conventional filter using the standard filter g-values according to [3]. The change of the cost function values with each iteration is shown in Fig. 6, converging at the 73th iteration. The optimization procedure is illustrated by the flowchart in Fig. 7. The optimized matrix is given in (16).

The corresponding S-parameter response and noise figure from both the optimized coupling matrix [m] and the initial coupling coefficient values are presented and compared in Fig. 8. It can be observed from Fig. 8(a) and (b) that the scattering parameters S_{11} and S_{22} display a Chebyshev filtering response simultaneously, and the gain in S_{21} is about 10 dB. The return losses seen from the input and the output of the amplifier are over 20 dB across the passband. The noise figure is calculated by substituting the submatrix of [m] into (14), and the response is shown in Fig. 8(c). The parameters related to the noise figure are Y_{opt}, NF_{min}, and R_N, and obtained via the EM simulation of transistor board in ADS. They are Y_{opt} = 0.0366+0.0148j S, NF_{min} = 0.5 dB, R_N = 3.05 Ω. It can be seen from Fig. 8(c) that both the calculated initial and optimized noise figures are very low over the passband. The noise figure of the optimized filter amplifier exhibits a wider bandwidth. The input impedance of the transistor versus frequency is shown in Fig. 8(d). Under the narrow band approximation, we assume the parameters of the transistor are constant and take the values at 10 GHz. After optimization, the coupling matrix achieves better shaped S-parameters response and a wider band noise figure matching. Note that in the optimization process, the targets are set to be Chebyshev matching and minimum noise figure. Practically, the they cannot be achieved simultaneously, nevertheless, a trade-off can be done by assigning appropriate values of weights of the cost-function.

B. Physical amplifier design using the Coupling Matrix

The amplifier structure is comprised of the SIW resonators, and the transistor mounted on a printed circuit board (PCB), as illustrated in Fig. 9. The transistor is connected to the input and output matching filters through dc-blocking capacitors. The transistor's input and output are directly coupled to Resonator 2 and Resonator 3 (Fig. 9). The couplings can be adjusted by the length of d_2 and d_3 (Fig. 9(a)). The input and output of the

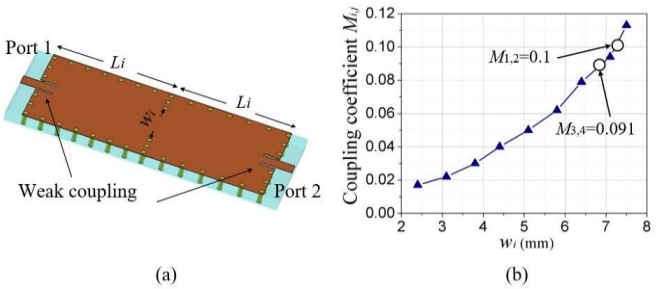

Fig. 10 Coupled SIW cavities used to extract the coupling coefficients. (a) Structure; (b) Coupling coefficients versus dimension w_1 and w_2. All points are at 10 GHz.

filter amplifier are 50 Ω transmission lines, and the external couplings are determined by d_1 and d_4.

The gaps d_1, d_2, d_3, and d_4 can be determined by extracting the external Q [26], calculated from the coupling coefficients in the matrix (16). Inter-resonator couplings $M_{1,2}$ and $M_{3,4}$ are determined by the size of the iris w_1 and w_2, as in a conventional filter. The values of the extracted external quality factor Q and coupling coefficients are calculated from the optimized coupling matrix as follows.

First, the inter-resonator couplings $M_{1,2}$ and $M_{3,4}$ are determined. $M_{1,2}$ and $M_{3,4}$ can be calculated by

$$M_{1,2} = FBW \cdot m_{1,2} \quad M_{3,4} = FBW \cdot m_{3,4} \tag{17}$$

In this example, $M_{1,2} = 0.1$ and $M_{3,4} = 0.091$. Two coupled SIW cavity resonators are simulated in the CST, as shown in Fig. 10(a). The coupling structures used provide weak couplings at the input and output ports. The coupling coefficient $M_{i,j}$ can be determined by adjusting the size of the coupling iris w_i. The relationship between w_i and the corresponding coupling coefficient $M_{i,j}$ is presented in Fig. 10(b), showing $w_1 = 7.15$ mm and $w_2 = 6.7$ mm can be found to fulfil the required $M_{1,2}$ and $M_{3,4}$.

The next step is to determine the external coupling structures d_1, d_2, d_3, and d_4. This can be done by extracting the external factor (Q_{ei}) of Resonator i (i = 1 to 4). Q_{ei} is related to the external coupling coefficients in the N+4 coupling matrix [25],

$$Q_{e1} = \frac{1}{FBW \cdot m_{P1,1}^2} \quad Q_{e2} = \frac{1}{FBW \cdot m_{2,in}^2}$$
$$Q_{e3} = \frac{1}{FBW \cdot m_{3,out}^2} \quad Q_{e4} = \frac{1}{FBW \cdot m_{P2,4}^2} \tag{18}$$

In addition, the center frequency (f_i) of the Resonator i (i = 1 to 4) can be determined by the self-coupling $m_{i,i}$ and is calculated by [26]

$$f_i = f_0 \left[\frac{FBW \cdot m_{i,i}}{2} + \sqrt{\left(\frac{FBW \cdot m_{i,i}}{2} \right)^2 + 1} \right] \tag{19}$$

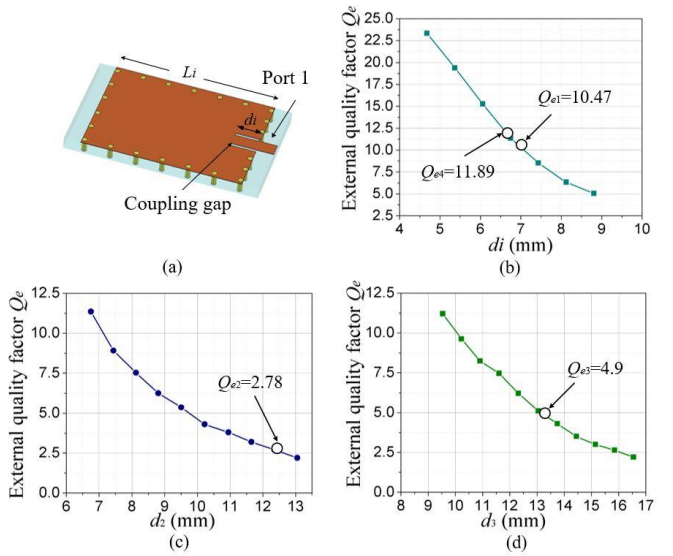

Fig. 11 (a) SIW structure used to extract external quality factor for Resonator 1 and 4. (b) External quality factors Q_e versus dimension d_1 and d_4. (c) Q_e versus d_2. (d) Q_e versus d_3.

TABLE II
DIMENSIONS OF INITIAL AND OPTIMIZED SIW FILTER-AMPLIFIERS (UNIT: MM)

	Initial	Optimized		Initial	Optimized
L_1	15.87	16.26	c_1	2.13	2.13
L_2	18.82	19.16	c_2	2.15	2.15
L_3	19.15	19.64	t_1	1.00	1.00
L_4	16.35	15.89	t_2	1.00	1.00
d_1	6.75	6.15	t_3	0.3	0.3
d_2	12.30	11.99	s	3.32	3.32
d_3	13.35	14.00	θ	75°	75°
d_4	6.50	6.33			
w_1	7.20	6.97			
w_2	6.80	6.87			
b_1	5.35	5.35			
b_2	5.13	5.13			

From (16), (17) and (18) the required external quality factors can be found to be $Q_{e1} = 10.47$, $Q_{e2} = 2.78$, $Q_{e3} = 4.9$, and $Q_{e4} = 11.89$. The center frequencies of the resonators are calculated as $f_1 = f_4 = 10$ GHz, $f_2 = 10.32$ GHz, $f_3 = 9.95$ GHz.

The external quality factor of the Resonator i (Q_{ei}) can be extracted from the simulation of the single SIW cavity. As illustrated in Fig. 11(a), with a weak coupling structure set up at port 1. The length of the coupling iris d_i is altered resulting in variations in external quality factor Q_{ei}. During the extraction process, the length of the resonator L_i is adjusted to keep the resonance at the center frequency f_i. The value of the Q_{ei} is plotted with different d_i in Fig. 11(b), (c), (d), and from these graphs we can find d_i for the external coupling iris of the SIW filter. Fig. 11(b) is used to determine the external a of the Resonator 1 and 4. L_i is adjusted to keep the center frequency at 10 GHz. Fig. 11(c) and (d) show the relationship between d_2 and d_3 and the external Q of Resonator 2 and Resonator 3. L_i is tuned to set the center frequency at f_2 = 10.32 GHz for Resonator 2 and $f_3 = 9.95$ GHz for Resonator 3.

Move onto the noise figure of the amplifier. In practical LNA design, power gain and optimal noise figure are a trade-off. A compromise has to be made. The primary aim of this work is to demonstrate the filter-amplifier with Chebyshev response for impedance matching using the N+4 coupling matrix. The noise figure has been optimized for NF_{min} over the passband and is

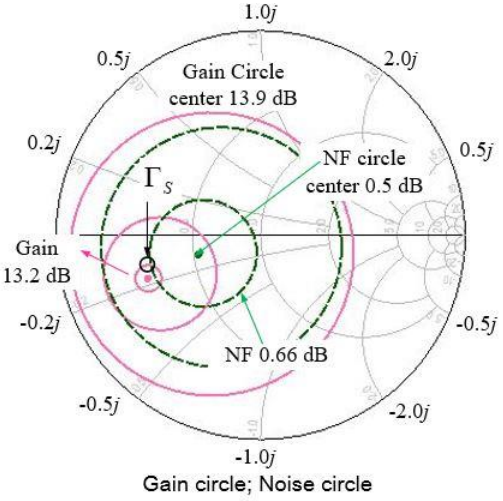

Fig. 12 Simulated gain and noise figure circles.

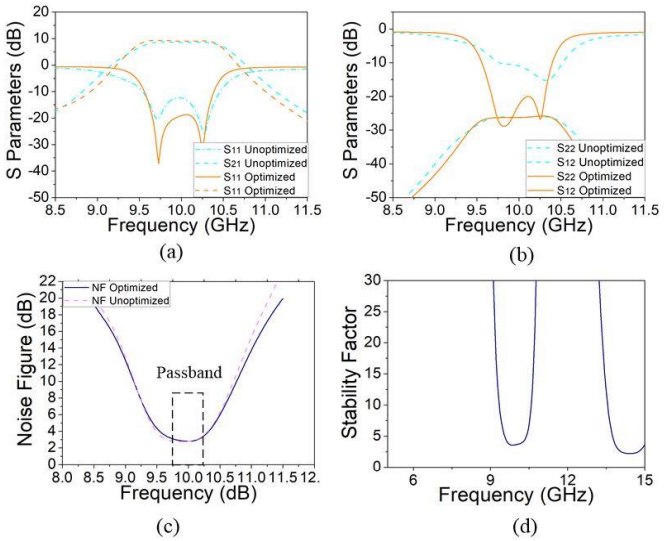

Fig. 13 Co-simulation results of the SIW filter-amplifier. (a) Scattering parameters S_{11}, S_{21}; (b) Scattering parameters S_{22}, S_{12}; (c) Noise figure; (d) Stability factors.

shown in Fig. 8(c). The EM simulation of the noise figure can be found using in ADS for verification and is shown in the Smith Chart in Fig. 12. This validates the noise figure calculation using the N+4 coupling matrix. The reflection coefficient looking into the source, Γ_S, is also identified on the Smith chart, at the point where the 13.2 dB gain circle and the 0.66 dB noise figure circle intersect.

After the initial values have been extracted, the whole filter-amplifier structure is simulated in CST. The simulated results before optimization are given in Fig. 13. After optimization using the EM simulator, better matching has been achieved as shown in Fig. 13. From Fig. 13(d), the simulated stability factors are all above 1, indicating the stability of the circuit from 5 GHz to 15 GHz. Note that the optimized results are close to the initial results, demonstrating the effectiveness of the parameter extraction technique. Table II gives the dimensions of the initial and the optimized filter-amplifier circuits.

V. Fabrication and Measurements

The SIW filter amplifier structure is fabricated from the Rogers RT/5880 substrate with a thickness of 0.508 mm and a relative dielectric constant of 2.2. The surface mount components are soldered on the PCB board manually. The connection wires provide dc-voltages at the gate and drain of the transistor. Both input and output are connected to the 50 Ω measurement ports through SMA connectors. Fig. 14 presents a photograph of the device. Conducting glue is used to align the PCB board with a CNC machined platform, which is used to fix the SMA connectors.

The Agilent vector network analyser PNA E8362B is employed for the *S*-parameters measurement. The bias conditions of the amplifier are V_{ds} = 2.45 V, and V_{gs} = -0.48 V. The measurement results are shown in Fig. 15 and are compared with the optimized simulated responses. Two poles are displayed in both S_{11} and S_{22} responses, indicating the

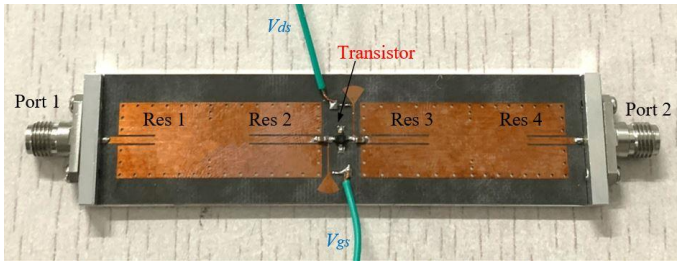

Fig. 14 Photo of the fabricated SIW filter amplifier.

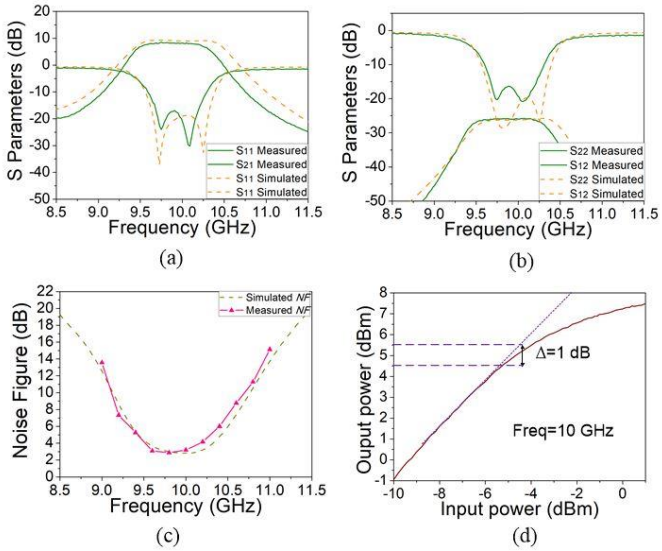

Fig. 15 EM simulation and measurement results. (a) Scattering parameters S_{11}, S_{21}. (b) Scattering parameters S_{22}, S_{12}. (c) Noise figure. (d) P1-dB measurement.

resonators at the input and output of the transistor work as second order filters. S_{21} shows about 9 dB gain over the passband. The measured input and output minimum return loss are around 17.7 dB and 16.5 dB respectively, over the passband. The measurement results agree well with the simulated response, validating the co-design approach of SIW filter-amplifier using N+4 active coupling matrix. The measured gain generally agrees with the calculated results of the coupling matrix, whereas in the previous work [24], the calculated gain is around 22 dB and the disagreement is large. This proves that the inclusion of the feedback coupling offers more accurate prediction of the amplifier performance. The noise figure is measured using a standard noise source and a spectrum analyser. A system amplifier with an all-band gain is employed to facilitate the measurement. The measured noise figure fits very well with the simulated response as shown in Fig. 15(c). In addition, the 1-dB compression (P1-dB) has been measured and is shown in Fig. 15(d).

The agreement between measurement and simulation is generally very good. The small disagreement may be caused by fabrication tolerance and unaccounted parasitic effects of the components. Surface mount capacitors are used to block dc at the expense of slightly degrading the gain of the transistor.

VI. Conclusion

In this paper, a coupling matrix based integrated filter-amplifier design technique is presented. The proposed N+4

matrix is more comprehensive than any of the previous matrix formulations for filter-amplifiers. It includes the feedback coupling, offering an accurate modeling for the transistor, which was neglected in previous work. The coupling matrix has also helped to extract more accurate initial values of the physical dimensions of the filter-amplifier, which can be used in full wave simulation and significantly improves the design efficiency.

The N+4 active coupling matrix is synthesized and used to obtain the S-parameters and noise figure of the amplifier. Based on a local gradient algorithm, matrix optimization can be rapidly performed, achieving amplification and Chebyshev filtering responses at the input and output ports simultaneously.

For the filter-amplifier verification, SIW filters are directly integrated to the input and output of a transistor. Complex impedances of the transistor can be directly matched by modifying the self-/external couplings terms in the proposed coupling matrix. The measured S-parameters response and noise figure fit well with the simulation, which validate the proposed coupling matrix technique.

With the transistor directly coupled to high-Q resonator-based filters, planar matching networks can be removed, hence lower loss and compact size can be achieved. As SIW passive components are widely studied and employed, this co-design technique of integrated multi-functional circuits of active and passive devices is expected to be of great value for compact integrated designs.

There are some limitations of the work. As the coupling matrix is synthesized under narrow band approximation, it would become less effective for wideband amplifiers. In our narrowband amplifier examples, the transistor is assumed to have frequency invariant input and output admittances.

The present design focuses on impedance matching and low noise figure of the amplifier. The active coupling matrix approach demonstrated here can be extended to other amplifiers with difference performance requirements such as power amplifiers and fix gain amplifiers. The cost function can be expanded to include more performance targets. The coupling matrix approach, with the help of non-resonance Y matrices, can be generalized to a wider range of microwave components, such as antennas, mixers, and multiplexers. It is expected that the technique described here can be extended to other multiple cascaded components and systems.

REFERENCES

[1] I. Bahl, Fundamentals of RF and Microwave Transistor Amplifiers. Hoboken, N.J.: Wiley, 2009.

[2] F. Schwierz, and J. J. Liou, *Modern Microwave Transistors: Theory, Design, and Performance*. New York, NY, USA: Wiley-Interscience, 2002.

[3] G. Gonzalez, Microwave Transistor Amplifiers: Analysis and Design. London, UK: Pearson, 1996.

[4] D. Pozar, Microwave engineering. Hoboken, NJ: Wiley, 2012.

[5] T. B. Kumar, K. Ma, and K. S. Yeo, "A 60-GHz coplanar waveguide-based bidirectional LNA in SiGe BiCMOS," *IEEE Microw. Wirel. Compon. Lett.*, vol. 27, no. 8, pp. 742-744, Aug. 2017.

[6] P. G. Courtney, J. Zeng, T. Tran, H. Trinh, and S. Behan, "120W Ka band power amplifier utilizing GaN MMICs and coaxial waveguide spatial power combining," *2015 IEEE Comp. Semi. Integ. Circ. Symp. (CSICS)*, New Orleans, LA, 2015.

[7] A. Aljarosha, A. U. Zaman and R. Maaskant, "A wideband contactless and bondwire-free MMIC to waveguide transition," *IEEE Microw. Wirel. Compon. Lett.*, vol. 27, no. 5, pp. 437-439, May 2017.

[8] D. Deslandes and Ke Wu, "Accurate modeling, wave mechanisms, and design considerations of a substrate integrated waveguide," *IEEE Trans. Microw. Theory Techn.*, vol. 54, no. 6, pp. 2516-2526, June 2006.

[9] X. Chen and K. Wu, "Substrate Integrated Waveguide Filters: Practical Aspects and Design Considerations," *IEEE Microw. Magazine*, vol. 15, no. 7, pp. 75-83, Nov.-Dec. 2014.

[10] X. Chen and K. Wu, "Substrate integrated waveguide filters: design techniques and structure innovations," *IEEE Microwave Magazine*, vol. 15, no. 6, pp. 121-133, Sept.-Oct. 2014.

[11] X. Chen and K. Wu, "Substrate integrated iaveguide filter: basic design rules and fundamental structure features," *IEEE Microw. Magazine*, vol. 15, no. 5, pp. 108-116, July-Aug. 2014.

[12] M. Bozzi, A. Georgiadis and K. Wu, "Review of substrate-integrated waveguide circuits and antennas," *IET Microw. Antennas Propag.*, vol. 5, no. 8, pp. 909-920, June 2011.

[13] A. A. Khan and M. K. Mandal, "A compact broadband direct coaxial line to SIW transition," *IEEE Microw. Wirel. Compon. Lett.*, vol. 26, no. 11, pp. 894-896, Nov. 2016.

[14] Ji-Xin Chen, Wei Hong, Zhang-Cheng Hao, Hao Li and Ke Wu, "Development of a low-cost microwave mixer using a broad-band substrate integrated waveguide (SIW) coupler," *IEEE Microw. Wirel. Compon. Lett.*, vol. 16, no. 2, pp. 84-86, Feb. 2006.

[15] A. A. Khan and M. K. Mandal, "Miniaturized Substrate Integrated Waveguide (SIW) Power Dividers," *IEEE Microw. Wirel. Compon. Lett.*, vol. 26, no. 11, pp. 888-890, Nov. 2016.

[16] F. Taringou, J. Bornemann and K. Wu, "Broadband coplanar-waveguide and microstrip low-noise amplifier hybrid integrations for k-band substrate integrated waveguide applications on low-permittivity substrate," *IET Microw. Antennas Propag.*, vol. 8, no. 2, pp. 99-103, 28 January 2014.

[17] K. K. Samanta, D. Stephens and I. D. Robertson, "60 GHz multi-chip-module receiver with substrate integrated waveguide antenna and filter," *Electronics Lett.*, vol. 42, no. 12, pp. 701-702, 8 June 2006.

[18] L. Chioukh, H. Boutayeb, K. Wu and D. Deslandes, "Monitoring vital signs using remote harmonic radar concept," *2011 41st European Microwave Conference*, Manchester, 2011, pp. 1269-1272.

[19] M. Abdolhamidi and M. Shahabadi, "X-Band Substrate Integrated Waveguide Amplifier," *IEEE Microw. Wirel. Compon. Lett.*, vol. 18, no. 12, pp. 815-817, Dec. 2008.

[20] Z. Wang and C. Park, "Novel substrate integrated waveguide (SIW)-based power amplifier using SIW-based filter to suppress up to the fourth harmonic," *2012 Asia Pacific Microw. Conf. Proc.*, Kaohsiung, 2012, pp. 830-832.

[21] K. Chen, J. Lee, W. J. Chappell, and D. Peroulis, "Co-design of highly efficient power amplifier and high-Q output bandpass filter," *IEEE Trans. Microw. Theory Techn.*, vol. 61, no. 11, pp. 3940-3950, Nov. 2013.

[22] K. Chen, T. C. Lee and D. Peroulis, "Co-design of multi-band high-efficiency power amplifier and three-pole high-Q tunable filter," *IEEE Microw. Wirel. Compon. Lett.*, vol. 23, no. 12, pp. 647-649, Dec. 2013.

[23] Y. Gao, J. Powell, X. Shang and M. J. Lancaster, "Coupling matrix-based design of waveguide filter amplifiers," *IEEE Trans. Microw. Theory Techn.* vol. 66, no. 12, pp. 5300-5309, Dec. 2018.

[24] Y. Gao, X. Shang, C. Guo, J. Powell, Y. Wang and M. J. Lancaster, "Integrated waveguide filter amplifier using the coupling matrix technique," *IEEE Microw. Wirel. Compon. Lett.*, vol. 29, no. 4, pp. 267-269, April 2019.

[25] R. J. Cameron, R. Mansour and C. M Kudsia, *Microwave Filters for Communication Systems: Fundamentals, Design and Applications*. 1st. New York, NY, USA: Wiley, 2007.

[26] J. S. Hong and M. J. Lancaster, *Microstrip Filters for RF/Microwave Applications*. New York, NY, USA: Wiley, 2001.

[27] K. Kurokawa, "Power waves and the scattering matrix," *IEEE Trans. Microw. Theory Techn.*, vol. 13, no. 2, pp. 194-202, Mar 1965.

[28] California Eastern Laboratories (2004, July). CEL Corp., CA. [Online]. Available: http://www.cel.com

Yang Gao was born in Henan, China, in 1992. He received the B.Eng. degree in telecommunication engineering from the Beijing Institute of Technology, Beijing, China, in 2014, and the Ph.D. degree in radio physics from the University of Birmingham, Birmingham, U.K., in 2018. After graduating from the University of Birmingham, he joined Zhengzhou University, Zhengzhou, China, as a Lecturer. In 2019, he was employed by the Department of International Cooperation, Ministry of Science and Technology of the People's Republic of China (MOST) on secondment. He is also an Honorary Research Fellow with the Emerging Device Technology Group, University of Birmingham. Yang's current research interests include integrated microwave-photonic circuits, passive/active devices and systems.

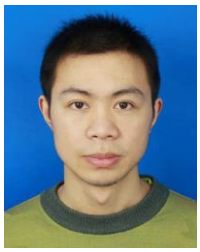

Fan Zhang was born in Sichuan, China. He is currently pursuing the Ph.D. degree in radio physics at School of Physics, University of Electronic Science and Technology of China, Chengdu, China.

From 2017 to 2018, he was a Visiting Student with University of Birmingham, Birmingham, U.K. His current research interests include design of microwave filters, 3-D printed filters, tunable filters, and millimeter-wave circuits.

Xin Lv (M'13) received the B.S., M.S., and Ph.D. degrees in electronic engineering from the Beijing Institute of Technology (BIT), Beijing, China, in 1982, 1988, and 1993, respectively. Since 1982, he has been a Lecturer, an Associate Professor, and a Professor with BIT, where he also serves as the Director of the Beijing Key Laboratory of Millimeter Wave and Terahertz Technique. His current research interests include millimeter-wave and terahertz circuits, antennas, and systems.

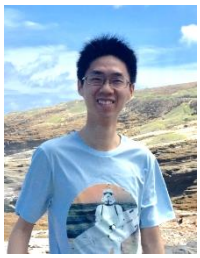

Cheng Guo was born in Chengdu, China, in 1990. He received the B.Eng. degree in communication engineering from Southwest Jiaotong University (Emei Campus), Chengdu, China, in 2012, and the Ph.D. degree in radio physics from University of Electronic Science and Technology of China (UESTC), Chengdu, China, in 2016. From 2014 to 2016, he was a visiting Ph.D. student of the University of Birmingham and a Research Fellow with the same university from 2017-2018. He is now an associate professor with School of information and communications engineering, Xi'an Jiao-tong university. His current research interests include 3-D printed passive microwave devices, Schottky diode-based THz frequency multipliers and mixers, as well as micromachined MMW/THz circuits. He is the recipient of the IEEE-MTTs Tatsuo Itoh Award in 2017.

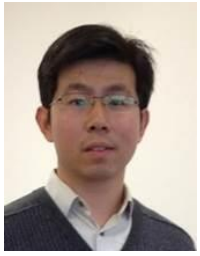

Xiaobang Shang (M'13–SM'19) was born in Hubei, China, in 1986. He received the B.E. degree (First Class) in electronic and communication engineering at University of Birmingham, Birmingham, U.K., in 2008, the B.E. degree in electronics and information engineering at Huazhong University of Science and Technology, Wuhan, China, in 2008, and the Ph.D. degree in microwave engineering at the University of Birmingham in 2011. His doctoral research concerned micromachined terahertz circuits and design of multi-band filters. He is currently a Senior Research Scientist with the National Physical Laboratory (NPL), Middlesex, U.K.. Prior to joining the NPL, he was a Research Fellow with the University of Birmingham. His current main research interests include microwave measurements, microwave filters and multiplexers, and micromachining techniques. Dr. Shang was the recipient of the ARFTG Microwave Measurement Student Fellowship Award in 2009, the co-recipient of the IEEE Microwave Theory and Techniques Society Tatsuo Itoh Award in 2017.

Lei Li received the B.S. degree in electronic engineering from Zhengzhou University, Zhengzhou, China, in 2004, and the Ph.D. degree in electronic engineering from the Institute of Acoustics, Chinese Academy of Sciences, in 2009. He is currently an Associate Professor with the School of Physics and Microelectronics, Zhengzhou University. His current research interests include array signal processing, optical gas sensing, and photoacoustic spectroscopy.

Jiashan Liu received the B.S. degree in electronic engineering from Beijing Institute of Technology, Beijing, China, in 2014. Currently, he is pursuing the Ph.D. degree at the school of information and electronics, Beijing Institute of Technology.

His research interests include millimeter-wave antennas and microwave passive components.

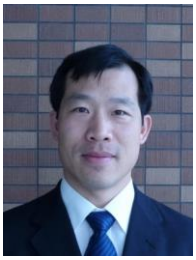

Yuhuai Liu was born in Anhui province in China in 1969. He received the B.Sc. degree in Physics in Anhui Normal University, and the M.Sc. degree and the Ph.D. degree in Optics in Anhui Institute of Optics and Fine Mechanics, Chinese Academy of Sciences (CAS) in 1996 and 1999, respectively. From 1999 to 2000, he worked in the Institute of Semiconductors of CAS in China as a post-doctor. He then worked as a research fellow in the University of Tokushima and Mie University in Japan from 2000 to 2007. He then joined Tohoku University as an assistant professor from 2007 to 2011, followed as a professor in Zhengzhou University till now. He is a visiting professor in Nagoya University from 2016. His research interests cover nitride semiconductors and optical communication. He has published 1 book chapter, 73 refereed journal papers and presented 137 conference reports.

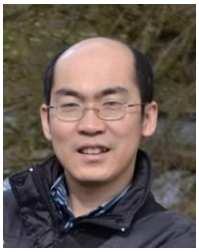

Yi Wang (M'09–SM'12) was born in Shandong, China. He received the B.Sc. degree in physics and M.Sc. degree in condensed matter physics at University of Science and Technology, Beijing, China, in 1998 and 2001, respectively, and the Ph.D. degree in electronic and electrical engineering at University of Birmingham, Birmingham, U.K., in 2005.

In 2011, he became a Senior Lecturer and then a Reader at University of Greenwich. In 2018, he joined the University of Birmingham as a Senior Lecturer. His current research interests include millimeter-wave and terahertz devices for metrology, communications and sensors, micromachining, microwave circuits based on multiport filtering networks, and filter-antenna integration.

Michael J. Lancaster (SM'2004) was born in York, England in 1958. He was educated at Bath University, UK, where he graduated with a degree in Physics in 1980. His career continued at Bath, where he was awarded a PhD in 1984 for research into non-linear underwater acoustics. After leaving Bath University where he graduated, he joined the surface acoustic wave (SAW) group at the Department of Engineering Science at Oxford University as a Research Fellow. The research was in the design of new, novel SAW devices, including RF filters and filter banks. In 1987 he became a Lecturer at The University of Birmingham in the Department of Electronic and Electrical Engineering, lecturing in electromagnetic theory and microwave engineering. Shortly after he joined the department he began the study of the science and applications of high temperature superconductors, working mainly at microwave frequencies. He was promoted to head the Emerging Device Technology Research Centre in 2000 and head of the department of Electronic, Electrical and Computer Engineering in 2003. He has published two books and over 200 articles in refereed journals. His current research interests include microwave filters and antennas and the high-frequency properties and the applications of a number of novel and diverse materials, which includes micromachining as applied to terahertz communications devices and systems.

Dr. Lancaster is a Fellow of the IET and the U.K. Institute of Physics. He has served on the IEEE MTT-S IMS Technical Committees.